*Friction* **12**(8): 1882–1896 (2024)
https://doi.org/10.1007/s40544-024-0890-7
ISSN 2223-7690
CN 10-1237/TH

RESEARCH ARTICLE

# The effect of electrical current on lubricant film thickness in boundary and mixed lubrication contacts measured with ultrasound

**Julio A. CAO-ROMERO-GALLEGOS[1], Saeid TAGHIZADEH[2], Oscar A. AGUILAR-ROSAS[1], R.S. DWYER-JOYCE[2], Leonardo I. FARFAN-CABRERA[1,*]**

[1] *Tecnologico de Monterrey, Escuela de Ingeniería y Ciencias, Ave. Eugenio Garza Sada 2501, Monterrey, N.L. 64849, México*

[2] *Department of Mechanical Engineering, Leonardo Centre for Tribology, University of Sheffield, Sheffield S1 3JD, UK*

*Received: 04 October 2023 / Revised: 25 January 2024 / Accepted: 03 March 2024*



**Abstract:** This work explores experimentally the effects of DC electrical currents on lubricant film thickness alteration in lubricated sliding steel contacts in the boundary and mixed regime as measured by ultrasound. The experiments were performed in a two-electrode cell-based pin-on-disk tester instrumented with ultrasonic transducers. Unelectrified and electrified tribological tests were conducted on steel flat-on-flat contacts under various speeds and loads using both a mineral base oil and a gear oil. Film thickness, coefficient of friction (CoF), and electrical contact resistance (ECR) were measured during short experiments (30 s) in unelectrified and electrified (1.5 and 3 A) conditions. The results suggest that film thickness, CoF, and all ECR are altered by passing DC currents through the contact. In particular, film thickness increased and decreased, respectively, by applying electricity at the different speeds and loads tested. These alterations were majorly ascribed to oil viscosity decrease by local heat and surface oxidation caused by electrical discharge and break down at the interface.

**Keywords:** electrified sliding; ultrasonic measurement; electric vehicles; pin-on-disk

## 1 Introduction

The passage of electricity through some tribological contacts, such as slip ring/commutators, catenary pantographs, and wheel/rail interfaces is essential for their function. However, electricity passing in bearings or gears from electric machines (motors and generators) is common but unwanted. It occurs due to stray currents coming from phenomena like magnetic flux asymmetry, inverter-induced voltages, and triboelectrification produced during the operation of electric machines [1, 2]. This has been demonstrated to be deleterious to the tribological performance of such elements, and has been widely reported [1, 3–7]. According to recent state-of-the art reviews [8, 9], electricity causes a variety of physical phenomena at metallic and non-aqueous lubricated contacts. Among the most critical mechanisms that affect friction and wear are; double-layer repulsion reducing the effective load (this is significant at very low contact pressures or at mixed and hydrodynamic lubrication regimes), charge-promoted adsorption, electrochemically driven oxide or additive films formation, and field-induced molecular rearrangement.

Recently, this subject has received renewed interest due to the increasing use of drivelines for electric vehicles and electricity generation equipment. Research has focused on the effects of electricity on surface tribo-chemistry and additive behavior [10–13], formation of metal oxides in dry and lubricated metal–metal contacts [14, 15], rolling contact fatigue promotion [16, 17], tribological behavior of new lubricants [18], and hard coatings/advanced materials [19]. In these investigations, analysis is based on determination

* Corresponding author: Leonardo I. FARFAN-CABRERA, E-mail: farfanl@tec.mx

of changes in friction coefficient, wear rates and mechanisms, contact temperature, lubricant degradation, tribochemistry of the contact surfaces, and sometimes contact resistance under external electric fields. All these phenomena depend on the formation of a lubricating film, but this is rarely measured directly. Lubricant film thickness depends upon many variables, such as type of lubricant (physicochemical properties), operating conditions (load and speed), stiffness, roughness, and texture of two contact surfaces, humidity, and temperature. There are various methods and techniques to measure the lubricant film thickness. These include electrical capacitance [20], electrical resistance [21], and eddy current methods [22, 23]. Their main disadvantage is noise generated and a need for a recess in the bearing load zone to mount the electrical probe [24]. Optical methods are also used to measure lubricant film thickness [25–29], although they require transparent windows which would insulate a contact. Contrastingly, ultrasound has been widely used to measure interfacial stiffness in dry and lubricated contacts and so deduce lubricant film thickness [30–36]. This technique is non-invasive, non-destructive and can measure the interface of the contacting parts inside a machine without insulating the contact, which is advantageous for electrified interfaces.

Although film thickness has been supposed to change by electrical current in previous research works [8, 9, 37], it has been scarcely demonstrated experimentally. Hence, this paper aims to provide a first experimental exploration of the film thickness alteration in sliding contacts in the boundary and mixed lubrication regimes due to external electrification in a two-electrode cell-based pin-on-disk tester instrumented with ultrasonic transducers.

## 2 Background

### 2.1 Reflection of ultrasonic waves from tribological contacts

When ultrasonic waves are incident at the boundaries of a medium or discontinuities, part of the ultrasonic energy is reflected, and part is transmitted. Provided the surface are smooth compared to the sound wavelength (and for practical bearing applications this is always the case) then there is no scattering of the wave at the rough surface contact. The reflection is caused by the difference in acoustic impedance of the contacting surfaces. For example, in a steel–air interface shown in Fig. 1(a), the acoustic impedance of the air is small compared to steel and almost all the incident wave amplitude is reflected [30]. As the air gaps in a solid–solid or a solid–lubricant–solid interface reduce when a contact is loaded, the ultrasonic wave reflection reduces (shown in Figs. 1(b) and 1(c)). The proportion of the wave amplitude reflection depends on the stiffness of the contact (which in turn depends on the materials and the real area of contact). Since part of the wave is transmitted through solid–solid or solid–liquid–solid conjunctions, these reflections are less than in a solid–air interface. The ratio of the reflected wave amplitude divided by the incident wave amplitude is known as the reflection coefficient. Since ultrasonic waves are almost completely reflected from a solid–air interface, in that reference case the incident wave is equal to the reflected wave. Thus, the reflection coefficient from a tribological contact is given by Ref. [30]:

$$R = \left| \frac{A}{A_{\text{ref}}} \right| \tag{1}$$

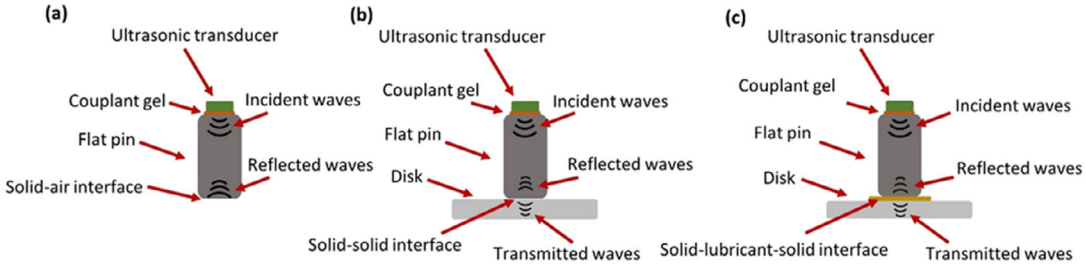


**Fig. 1** Schematic diagram of ultrasonic waves reflected from: (a) solid–air interface where there is almost complete reflection, and the incident wave equals the reflected wave; (b) solid–solid contact (dry contact) where some sound is transmitted through the contact regions; (c) solid–lubricant–solid contact (lubricated contact) where sound is transmitted through both solid contacts and lubricant film.

where $A$ is the amplitude of the reflected wave from the tribological contact and $A_{ref}$ is the amplitude from the solid–air interface (the reference interface).

### 2.2 Oil film thickness measurement using ultrasound

Figure 2 shows a schematic diagram of the flat contact between a pin and disk interface under normal load. In the absence of lubricant, real contact occurs at the asperities, as shown in Fig. 2(b). The contacting surfaces are separated by the mean lines of the roughness (surface separation) of both surfaces $h$. The rougher the surfaces are, the larger the separation. Figure 2(c) shows a boundary contact where the interface is partly made by solid–solid contact and the gaps in the roughness are filled by lubricant (Fig. 2(c)). As sliding takes place, a hydrodynamic film starts to form, the contacting surfaces are separated by more lubricant, and fewer asperity contacts occur; this is known as mixed lubrication (Fig. 2(d)). For the purposes of studying the response of an ultrasonic wave, the contact can be modeled as two springs in parallel [38] (Fig. 2(e)); a solid spring and a liquid spring. The reflection coefficient, $|R|$, can be calculated using the interfacial stiffness of the combined springs in parallel, $K_{tot}(=K_s+K_l)$, according to the well-known spring model for reflection [39, 40]:

$$|R|=\frac{1}{\sqrt{1+\left(\frac{2K_{tot}}{\rho_s c_s \omega}\right)^2}} \tag{2}$$

where $\omega$ is the angular frequency of the incident wave, and $\rho_s$ and $c_s$ are the density of the solid media and the speed of sound in the solid media, respectively. This is rearranged to give the combined interface stiffness:

$$K_{tot}=\frac{\rho_s c_s \omega}{2}\frac{\sqrt{1-|R|^2}}{|R|} \tag{3}$$

For a purely dry contact (the lubricant spring is absent, $K_l = 0$), the interfacial stiffness is given by

$$K_s=\frac{\rho_s c_s \omega}{2}\frac{\sqrt{1-|R_s|^2}}{|R_s|} \tag{4}$$

where $R_s$ is the reflection coefficient of dry contact. The interfacial stiffness in the boundary and mixed lubrication is the sum of the solid interfacial stiffness $K_s$ and the lubricated interfacial stiffness $K_l$ as shown in Fig. 2(e). These stiffnesses are in parallel since the contact pressure is carried simultaneously by both the asperities and lubricants. The stiffness of the oil film alone is then given by [35]:

$$K_l=K_{tot}-K_s \tag{5}$$

The stiffness of a lubricant film is related to its film thickness and bulk modulus according to [36]:

$$K_l=\frac{B}{h} \tag{6}$$

The bulk modulus $B$ (reciprocal of the compressibility) can be expressed in terms of the lubricant density $\rho_l$, and speed of sound in the lubricant $c_l$ [36] and so:

$$h=\frac{\rho_l c_l^{\,2}}{K_l} \tag{7}$$

The speed of sound in the oil in the bulk is measured (Table 2), although it should be noted that it is hard to know the composition exactly of the oil that actually exists in the asperity gaps. In the boundary and mixed lubrication, the surface separation (the distance between the mean lines of the two rough surfaces) and the lubricant film thickness are equal [35]. The thinner the lubricant layer is, the stiffer the interface. However, the proportion of the solid and lubricated contact in both boundary and mixed lubrication is unknown. Therefore, it is difficult to distinguish the portion of reflected ultrasonic waves that comes from the solid and lubricant part. To address this limitation, the total stiffness of a lubricated contact ($K_{tot}$ in Eq. (3)) and the stiffness of a dry contact ($K_s$ in Eq. (4)) are measured separately. The stiffness of the lubricant alone is then determined by substituting the dry and total contact stiffnesses into Eq. (5). This tacitly assumes that the stiffness of a dry contact is the same as the stiffness of the asperity part of a mixed lubricated contact (under the same loading conditions). The oil film thickness is then obtained using Eq. (7).

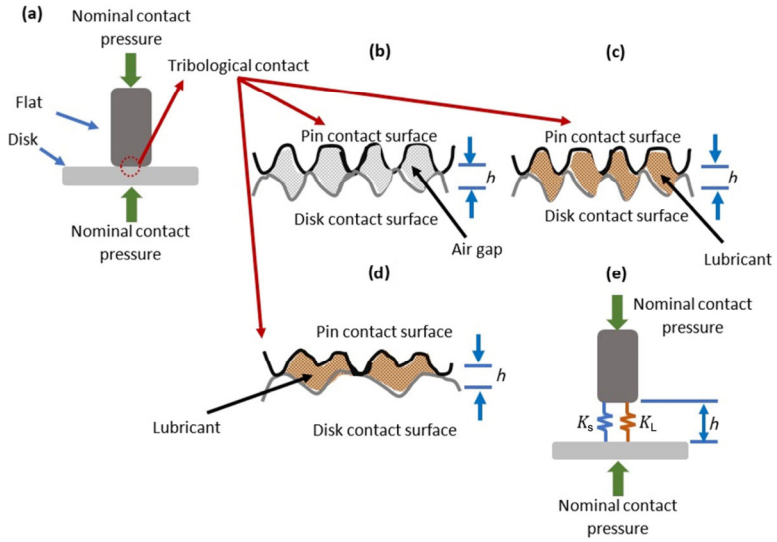


**Fig. 2** Schematic diagram of tribological contacts under a nominal applied contact pressure: (a) flat pin–disk contact; (b) dry contact; (c) boundary lubrication contact; (d) mixed lubrication contact; (e) equivalent spring model.

## 3 Experimental details

### 3.1 Specimen loading and test apparatus

Figure 3 shows a schematic of the contact loading and test apparatus. A flat-ended pin is loaded against a rotating disk in a Bruker UMT-3 tribometer. The contact was run either dry or fully immersed in a lubricant (about 20 mL) in the disk holder. The pin and disk were electrically isolated from the housing and carbon brushes were used to conduct the rotating disk component.

Two test procedures were used to identify the film thickness variation with speed and load by electrification. Firstly, a speed sweep, where a constant load of 50 N was applied while the disk was rotated at a rotational speed increasing from 20 rpm to 90 rpm. Then a second set, where a constant rotational speed of 50 rpm was applied while the normal load on the pin was increased from 10 N to 80 N. For both sequences, reflected ultrasonic signals from the dry and lubricated contacts both with and without applying electrical currents to the contact were recorded.

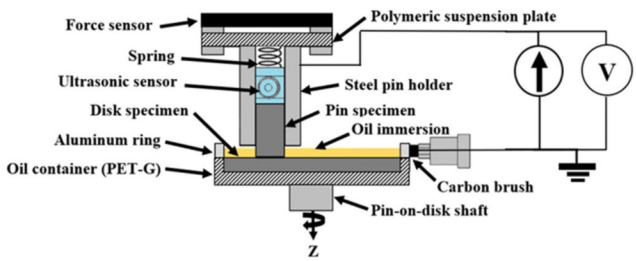


**Fig. 3** Two-electrode cell-based pin-on-disk set-up instrumented with ultrasound equipment for running unelectrified and electrified sliding tests and measuring film thickness.

### 3.2 Electrical apparatus

To induce external DC electricity (a constant current with variable voltage depending on the contact resistance variability) to the sliding contact during the test, a DC power supply was connected on one side to the pin steel holder, which was in contact with the pin, and the other side to a carbon brush, which in turn slid over an aluminum ring fixed to the plastic oil container and connected to the disk sample. To provide proper electrical insulation and avoid electricity passing to the tester´s sensors, the disk holder was 3D printed (100% infill) with (PET-G) while the pin holder made of steel was attached to a suspension polymeric plate (an accessory of the test machine) which provided electrical insulation. In order to have an insight on possible tribo-chemical changes occurring at the interface during sliding, an ohmmeter datalogger was connected to the pin and carbon brush to measure directly the electrical contact resistance (ECR) variation with sliding distance for the unelectrified tests. On the other hand, a voltmeter datalogger was used to measure the variation in voltage $V$ with test time for the electrified tests (much higher external DC current applied), and then calculate

the variation in ECR with the applied constant current, I, through Ohm´s law (see Eq. (8)).

$$\mathrm{ECR} = \frac{V}{I} \tag{8}$$

It is noteworthy that ECR measurement by any Ohmmeter requires the application of a low DC current (0.01–0.05 A) for non-electrified externally electrified contacts. In this case, the implemented voltmeter applied a DC current of 0.01 A for measuring ECR in the unelectrified tests. This low current was found in preliminary testing to effectively measure ECR and generate no changes in CoF and wear for the lubricated steel interfaces in comparison to those not connected to an ohmmeter.

### 3.3 Ultrasonic instrumentation

As shown in Fig. 3, a piezoelectric longitudinal transducer (10 mm diameter) with a peak frequency of 3 MHz was attached (using a coupling gel) to the back face of the pin. The transducer both emitted and received reflected signals from the pin–disk contact in both dry and lubricated cases. A 3 MHz longitudinal ultrasonic wave with 3-tone burst cycles at a peak-to-peak incident voltage of 90 V was generated using a high-power amplifier (RITEC RAM-5000). A reference signal was recorded from the pin–air interface. A PC equipped with LabView was used to trigger and digitize the reflected ultrasonic waves from the contact. The accuracy of the ultrasonics method for measuring oil film thickness in metal interfaces have been reported elsewhere [30–33].

### 3.4 Test specimens

A flat pin (diameter 6 mm and length 20 mm) and disk (diameter 60 mm and thickness 10 mm) made of steel C40 were used. The contact surfaces were polished with silicon carbide papers to P800 grit size. The surface roughness (arithmetic mean deviation $R_a$ and root mean square $R_q$) was measured using an optical profilometer (Alicona Infinite Focus SL) according to ISO 4287 as shown in Table 1.

Two different lubricants were used to investigate the effect of lubricant type on the electrical sensitivity. Table 2 shows the properties of the lubricants and specimens. Densities and kinematic viscosities are displayed as reported from the supplier's data sheets. Time of flight (TOF) was used to measure the speed of sound in the oils. To do this, two transducers were placed on two end ends of a cylinder to work in a through transmission mode. At the peak frequency of 3 MHz and amplitude of 90 V, the distance between the emitter and receiver varied, and propagated ultrasonic waves were captured. By knowing the distance between the transducers and the time of flight, the speed of sound in the oils were determined as shown in Table 2.

**Table 1** Surface roughness of the flat pin and before and after the friction tests.

| Specimen | Process | $R_a$ (μm) | $R_q$ (μm) |
|---|---|---|---|
| Flat pin | Before test | 0.730±0.252 | 0.95±0.381 |
| | After test | 3.247±0.641 | 4.338±0.869 |
| Flat disk | Before test | 1.486±0.171 | 1.901±0.271 |
| | After test | 2.126±0.719 | 2.784±0.516 |

**Table 2** Properties of the lubricants and solid materials used in this study.

| Test material | Density, $\rho$ (kg/m$^3$) | Kinematic viscosity at 40 °C/100 °C (cSt) | Speed of sound, $c$ (m/s) at room temp. |
|---|---|---|---|
| Gear oil | 889.0 | 147.2/15.2 | 1584 |
| Mineral oil | 849.2 | 42.0/6.5 | 1468 |
| Flat pin/disk | 7800 | — | 6400 |

### 3.5 Test conditions

The tribological testing conditions are given in Table 3. To determine the change in film thickness by inducing DC under different conditions, the electrical current, load, and speed were varied. In total, 12 sets of tests were carried out by varying load (load sweep) and speed (speed sweep) for both oils and under different electrical currents (0, 1.5, and 3 A) in order achieve boundary and mixed lubrication regimes. The selected current magnitudes were intended to replicate the peak values of stray currents (~1.4 A) reported for high power induction motors (1.5 kW) [41] and to generate significant alteration in CoF and wear of the tribopair tested. Friction coefficient, electrical resistance, and ultrasonic reflection were measured simultaneously during the 30 s duration of each test. It should be noted that the tests run at 0 A were actually conducted

**Table 3** Tribological testing conditions.

| Test set | Lubricant | Speed (m/s) | Load (N) | DC current (A) |
|---|---|---|---|---|
| Speed sweep | Gear oil (GO), mineral base oil (MBO) | 0.06, 0.08, 0.12, 0.16, 0.18, 0.2, 0.24, 0.28 | 50 (constant) | 0, 1.5, 3 |
| Load sweep | Gear oil (GO), mineral base oil (MBO) | 0.16 (constant) | 10, 20, 30, 40, 50, 60, 70, 80 | 0, 1.5, 3 |

under the very low current (0.01 A) applied by the Ohmmeter connected to measure ECR. In pretrials, it was found that <0.1 A generate negligible changes in CoF, film thickness and wear for the conditions and tribopair tested, so the current applied by the Ohmmeter to measure ECR was considered as unelectrified condition. The same pin and disk pair were used to run three repeats of each test condition. Before starting each test, the specimens were subjected to a running-in process in the tester to pair and align the contacting surfaces appropriately (pin specimen sliding on a polishing paper mounted in the oil container, and further dry sliding with actual testing specimens). According to the flat-on-flat contact configuration, the pressures ranged between ~0.35 MPa and ~3 MPa at the minimum and maximum loads tested.

### 3.6 Signal processing

Figure 4(a) shows an example reflected wave signal in the time domain from a solid–air and a lubricated interface. The reflected signal from the solid–air interface is used as a reference signal as explained in Section 2.2. Two groups of reflections can be seen and are indicated on the figure: the first echo from the interface and the second.

In this study, only the first reflected signals were used for the analysis. These first reflected signals were averaged over 50 signals followed by extraction using a Hanning window and a zero-pad function to improve the resolution of the signals as shown in Fig. 4(b).

To determine the reflection coefficient the amplitude of the reflected ultrasonic waves at the incident frequency is needed. This can be difficult to distinguish in the time domain, so a fast Fourier transform (FFT) was applied as shown in Fig. 4(c). The peak at the fundamental frequency (just over 3 MHz) of the solid–air and lubricated contact reflections, as shown in Fig. 4(c), correspond to the amplitude of the reference ($A_{ref}$) and lubricated contact ($A$), respectively. These values are substituted into Eq. 1 to determine the reflection coefficient of the dry and lubricated contact for each test case.

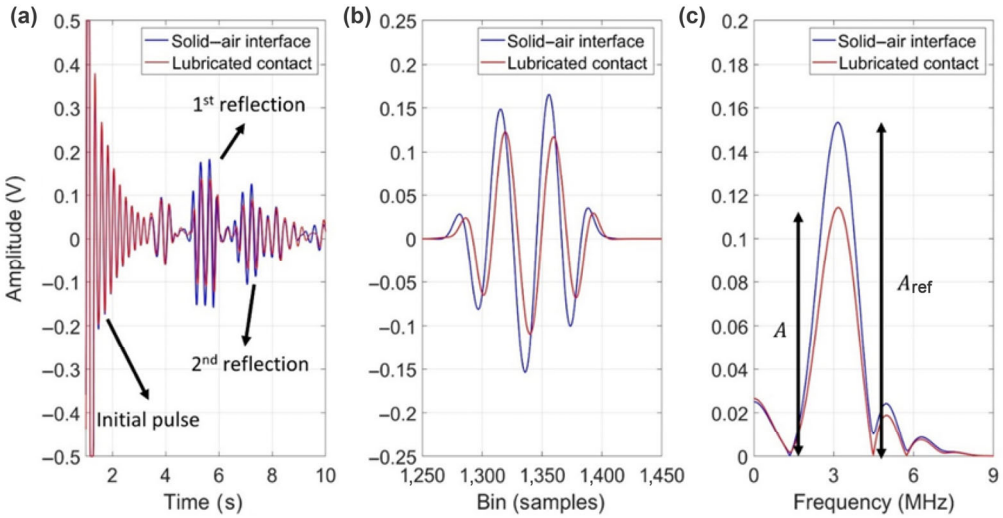


**Fig. 4** Signal processing of the reflected pulses from a solid–air and lubricated contact with gear oil using 90 V excitation with incident frequency 3 MHz under 50 N at 50 rpm in the absence of electricity: (a) time domain signals; (b) hanning window and zero pad results of the first reflected waves packet; (c) fast Fourier transform (FFT) results of the first reflected signal.

## 4 Results and discussion

### 4.1 Reflection coefficient and interface stiffness

Figures 5(a), 5(c), 6(a), and 6(c) show the reflection coefficient of dry and lubricated contacts with gear oil and mineral oil obtained in the speed and load sweep tests, respectively. These reflection coefficients are substituted into Eqs. (3) and (4) to determine the total and dry interfacial stiffnesses as shown in Figs. 5(b), 5(d), 6(b), and 6(d).

In each case, the dry contact reflects more ultrasound than the lubricated case; the lubricant filled voids provide a better sound path than air filled voids. It follows that the dry contact is less stiff than the lubricated case. For the dry contact the interface stiffness arises from the stiffness of the asperity contacts alone. The air between the asperities contacts has negligible stiffness. For the lubricated case the stiffness arises from these asperity contacts and the stiffness of the pockets of oil in the gaps between the contacts. So, the stiffness is higher, as the air gaps are now filled with lubricant which has a bulk modulus many times greater than that of air. The stiffness is then the combined stiffness of solid and liquid springs in parallel. Reference [35] describes work where this phenomenon of combined liquid and solid stiffness in the mixed lubrication regime is explored in detail.

It is also observed from Figs. 5(b), 5(d), 6(b), and 6(d) that as the electric current increases, the contact tends to become stiffer. It was more evident in the speed sweep tests, see Figs. 5(b) and 6(b). This stiffness behavior may be since electrification of dry and lubricated sliding steel interfaces promotes accelerated metal oxidation [3], which forms metal oxide products/layers at the interface, and consequently increasing film thickness stiffness.

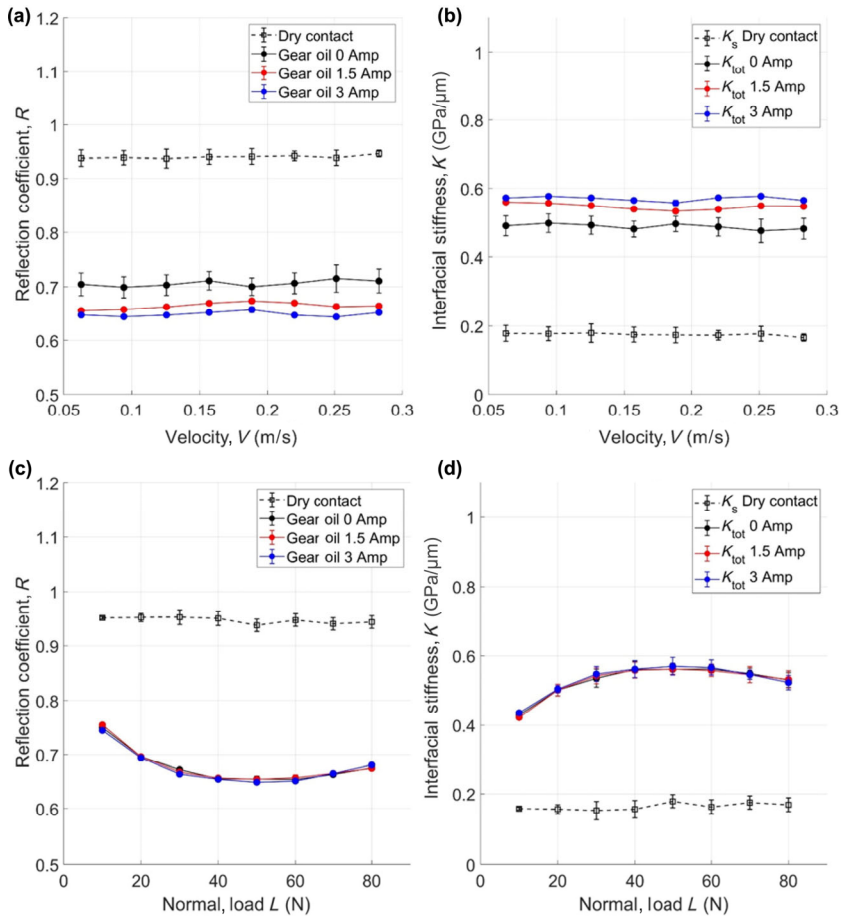


**Fig. 5** Signal processing of reflected signals from dry and lubricated (gear oil) contact: (a) reflection coefficient as a function of speed; (b) interfacial stiffness as a function of speed; (c) reflection coefficient as a function of load; and (d) interfacial stiffness as a function of speed.

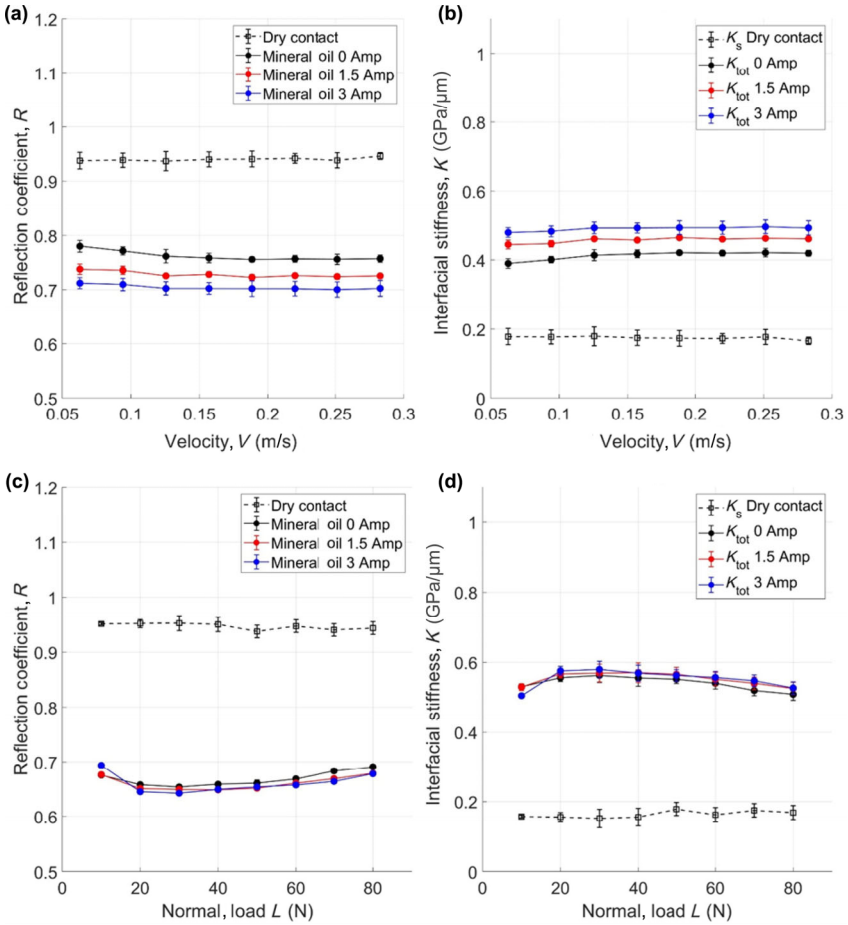


**Fig. 6** Signal processing of reflected signals from dry and lubricated (mineral oil) contact: (a) reflection coefficient as a function of speed; (b) interfacial stiffness as a function of speed; (c) reflection coefficient as a function of load; and (d) interfacial stiffness as a function of normal load.

### 4.2 Oil film thickness variation

Substituting the dry contact stiffness, $K_s$ and the total interfacial stiffness $K_{tot}$ into Eq. (5) gives the liquid stiffness, $K_l$ and this into Eq. (7) gives the oil film thickness, $h$. The resulting oil film thickness for the speed and load sweeps are shown in Figs. 7 and 8, respectively. It can be seen that there was not a significant change in film thickness when varying speed for both oilsunder unelectrified condition. However, a more evident difference was found when varying load (see Figs. 8(a) and 8(b)). The gear oil film thickness is slightly larger, since the viscosity is greater. A slight film thickness increase (about 1 μm) in the load ramp test was found after 40 N for both oils, which is unexpected but within the accuracy of the measurement method. It is possibly related to more wear (increase in roughness) caused by higher contact pressures. The higher roughness in the contact means a less stiff interface which would appear as a slight increase in the film thickness.

It is seen from Fig. 7, as the electrical current increases, the oil film thickness decreases. The minimum oil film thickness was created when the oils were subjected to 3 A. In all cases the oil film thickness ($\sim 3\,\mu m < h < \sim 9\,\mu m$) is close to the combined surface roughness of the pin and disk as shown in Table 1 ($0.951\,\mu m < h < 2.851\,\mu m$) indicating the boundary and mixed lubrication regimes. The oil film thickness slightly decreases as the speed increases. Hydrodynamic effects are marginal, and as the speed increases, the temperature of the lubricant increases. This would reduce the lubricant viscosity and subsequently a reduction in the film thickness.

The film thickness reduction with electric current obtained for both oils is clear for both oils. This is ascribed to i) oil viscosity reduction due to heat

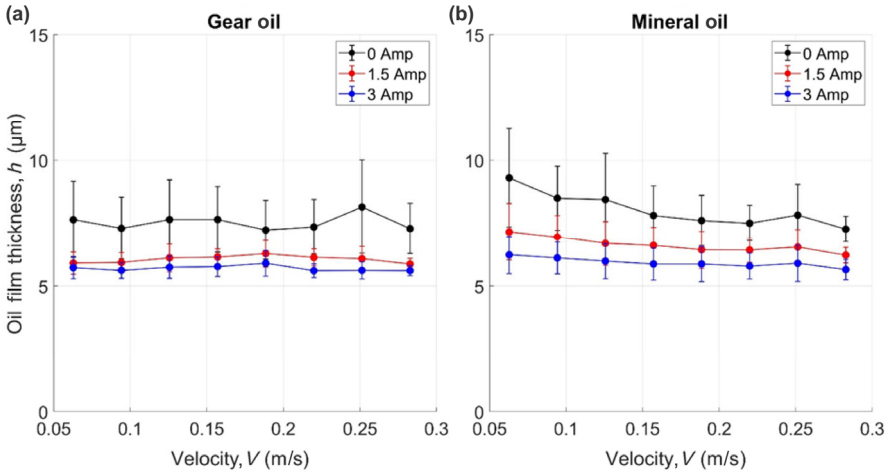


**Fig. 7** The oil film thickness as a function of the speed of flat pin under 50 N normal load: (a) gear oil and (b) mineral oil.

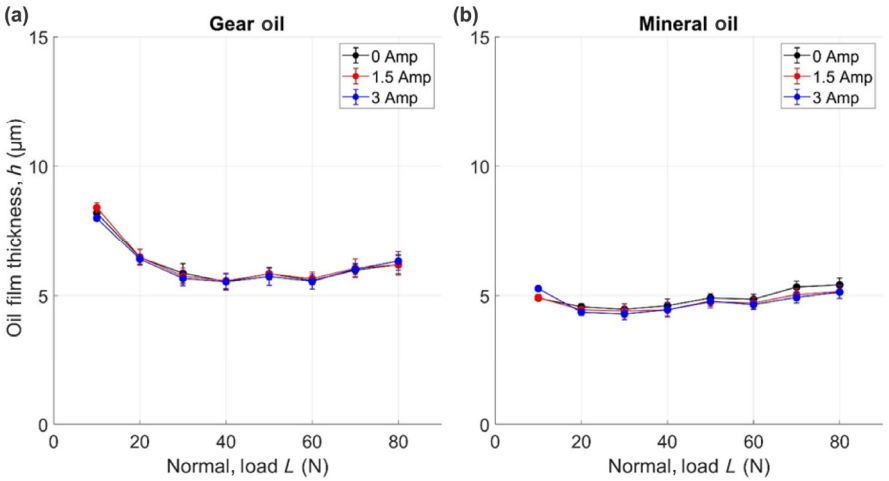


**Fig. 8** An oil film thickness as a function of the normal load of flat pin under 0.157 m/s speed: (a) gear oil and (b) mineral oil.

increase by electrical discharge and breakdown at the interface; and ii) metal oxidation layer formation at the interface, as illustrated in Fig. 9. As found in previous research works [3, 4, 42, 43], the magnitudes of electrical currents applied in the tribo-pair quickly form metal oxidation at the interface. The film thickness reduction with electricity is less evident for the load sweep tests (see Fig. 8). It may be because the oil viscosity reduction by heat during electrification has less influence in the film thickness by increasing load than varying speed (constant load) or the oxide layer is removed by increasing load.

### 4.3 Coefficient of friction (CoF) and electrical contact resistance (ECR)

The coefficient of friction (CoF) and electrical contact resistance (ECR) obtained for mineral oil and gear oil during the unelectrified and electrified tests are shown in Figs. 10–13. Figures 10 and 11 show the results obtained for the speed sweep while Figs. 12 and 13 show the results for the load sweep. ECR behavior is useful to have an insight about the interface

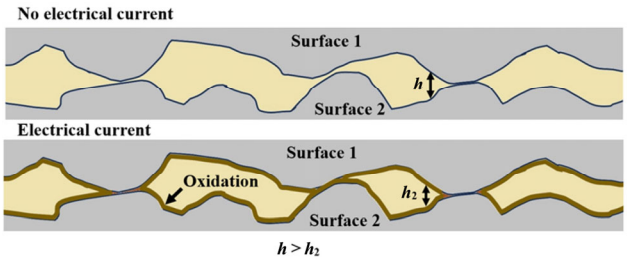


**Fig. 9** Illustration of sliding surfaces asperities showing the generation of an oxide layer produced by applying an electrical current.

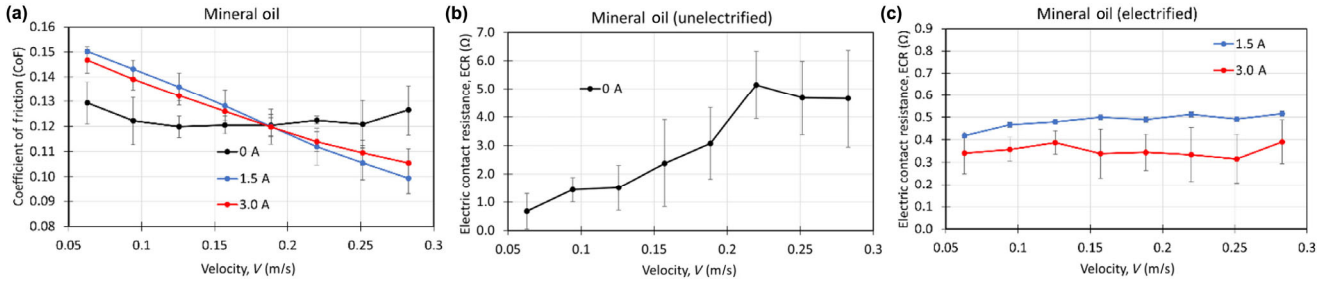


**Fig. 10** (a) coefficient of friction (CoF) for mineral oil in the speed sweep tests; (b) electrical contact resistance (ECR) under unelectrified condition; (c) electrical contact resistance (ECR) under electrified tests.

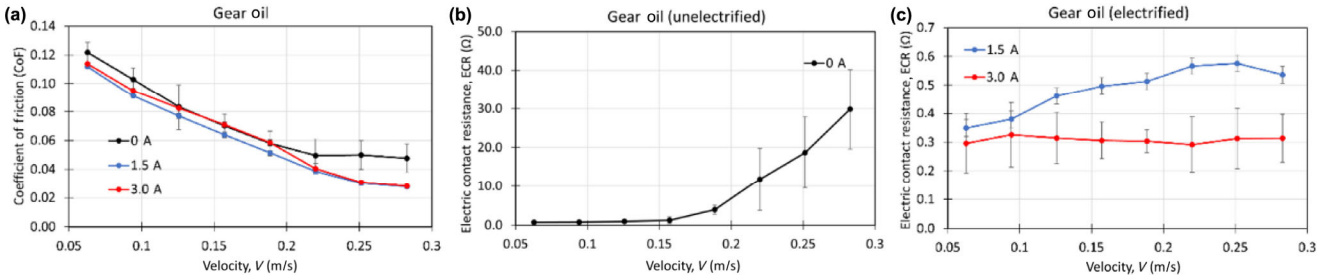


**Fig. 11** (a) coefficient of friction (CoF) for gear oil in the speed sweep tests; (b) electrical contact resistance (ECR) under unelectrified condition; (c) electrical contact resistance (ECR) under electrified tests.

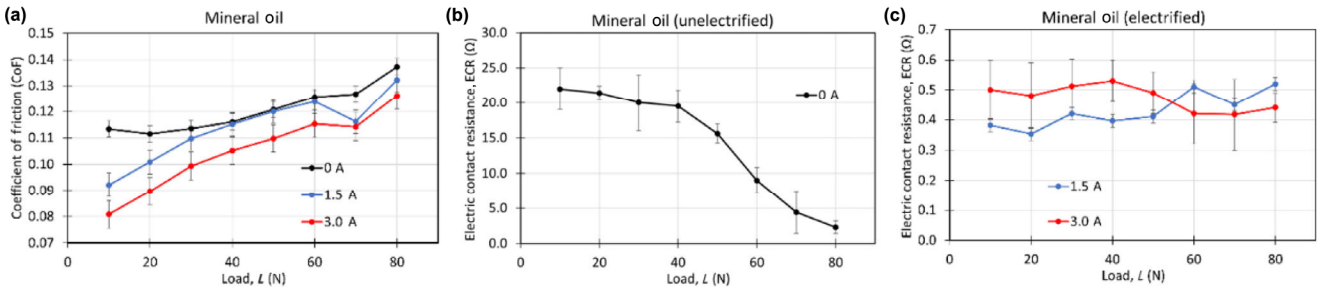


**Fig. 12** (a) coefficient of friction (CoF) for mineral oil in the load sweep tests; (b) electrical contact resistance (ECR) under unelectrified condition; (c) electrical contact resistance (ECR) under electrified tests.

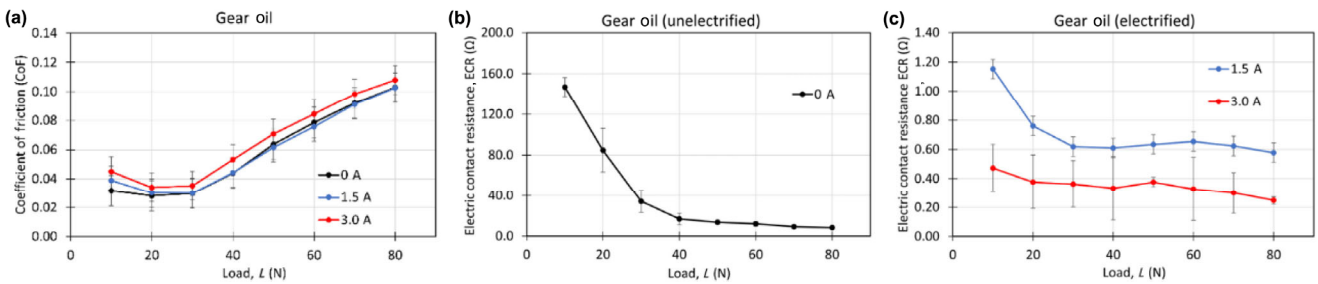


**Fig. 13** (a) coefficient of friction (CoF) for gear oil in the load sweep tests; (b) electrical contact resistance (ECR) under unelectrified condition; (c) electrical contact resistance (ECR) under electrified tests.

condition. One can assume changes in real contact area caused by wear and formation of chemical compounds with different resistivity at the interface.

For the speed sweep (Figs. 10 and 11), the CoF tended to remain constant with speed for mineral oil and to decrease for gear oil under unelectrified condition, see Figs. 10(a) and 11(a). The CoF decrease obtained for gear oil is possibly caused by the activation of additives in the formulation due to the heat and shear stress increase at rising speed [44]. In the case of the electrified condition, CoF decreased with speed for both oils. It can be ascribed to the

possible formation of metal oxide products/layer by electrification, which can act as a solid lubricious layer. The oxide products/layer formation is assumed because film thickness reduced with electrification, as depicted in Fig. 7.

In an ideal tribological contact (constant speed, temperature, and load), it might be expected that ECR should reduce with sliding progression since the real contact area increases facilitating passage of electric current. However, in these experiments, ECR increased with speed for both oils under unelectrified condition, see Figs. 10(b) and 11(b). It is because the asperities contact at the interface becomes more intermittent by increasing speed and thus electrical contact. ECR for electrified tests also increased marginally with speed, seeing Figs. 10(c) and 11(c). Additionally higher electrical resistance arises due to the formation of metal oxides which have higher resistivity than steel (i.e., hematite oxide resistivity is about $10^6$ Ω·cm [45] while steel resistivity is in the order of $10^{-4}$ Ω·cm). In general, ECR magnitudes under electrification were significantly lower than those under unelectrified condition. This is because increasing the applied external electrical current (DC) reduces the electrical potential required, and thus, ECR decreases as ruled by the Ohm's law (see Eq. (8)). The variation or error in ECR was large for most of the cases, especially when varying sliding speed, since electrical conductivity interference occurs through the sliding. Besides, ECR standard deviation varied greatly under unelectrified conditions for both oils. This is because much larger currents (1.5 and 3 A) are applied under electrified condition in contrast to that unelectrified in which the Ohmmeter applies only 0.01 A. Larger currents promotes less electrical conductivity interference in a sliding contact.

For the load sweep (Figs. 12 and 13), CoF tended to increase with load for both oils under both unelectrified and electrified conditions. This CoF increase can be related to the decrease of film thickness (as seen in Fig. 8) and increase in solid contact with load. In the case of mineral oil, CoF reduced with electrical current meanwhile it increased for gear oil, as also found in a previous research work using similar oils [42]. These CoF alterations by electrification are related to the chemical nature (additive content) of each oil. Electrical current may promote adsorption/desorption of polar additives and boost the stimulation or suppression of redox reactions at the contact interface varying CoF differently than base oils [8]. ECR decreased with load under unelectrified condition for both oils, seeing Figs. 12(b) and 13(b), as expected due to the increase in real contact area by the contact pressure increase. In the case of electrified condition, ECR exhibited a slight increase with load for mineral oil but a decrease for gear oil, see Figs. 12(c) and 13(c). The decrease of ECR for gear oil is related to the real contact area increase with load, but also to the film thickness decrease with load, as presented in Fig. 8. On the other hand, the ECR increase with load obtained for mineral oil under electrification is again associated to the possible formation of metal oxides at the interface, which have higher resistivity than the steel interface. In this way, ECR tend to keep constant or even increase with load instead of decrease. The mineral oil lubricated contact can be more prone to producing metal surface oxidation due to the lack of additives which protect the metal surface against oxidation.

### 4.4 Surface analyses

To find evidence of the formation of oxide products/layer in the sweep tests, in which film thickness exhibited significant reduction by electrification, the pin sample surfaces used for electrified (3A) tests were analyzed by Raman spectroscopy. The spectra obtained under unelectrified and electrified conditions using mineral oil and gear oil are shown in Figs. 14(a) and 14(b), respectively. The Raman bands found corresponded mainly to those bands of the hematite ($\alpha$-$Fe_2O_3$) type oxide (226, 291, 406, 498, 658, and 1,320 $cm^{-1}$) [46], as similar to that reported elsewhere [3]. The hematite bands for the electrified condition (3A) were found to be more intense than those from unelectrified (0 A) condition. It can confirm that oxidation was more severe after passage of electricity and being able to form more oxide products or thicker oxide layers at the steel interface than unelectrified tests.

Finally, the alteration of film thickness in steel/steel contacts under electrical conditions was found to be a complex problem involving many variables, which require different systematic experiments to get a

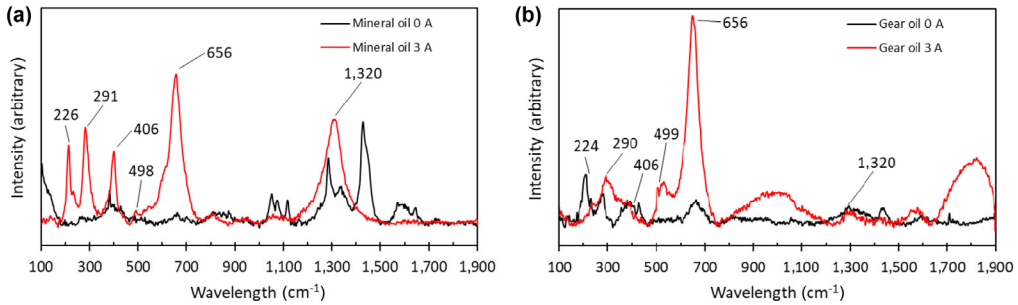


**Fig. 14** Comparison of Raman spectra obtained from the pin samples surfaces after the speed sweep tests under unelectrified and electrified conditions for: (a) mineral oil; (b) gear oil.

total comprehension. Within this first experimental approach, the authors found lubricant local heating and surface oxidation as the most notable sources of film thickness alteration, confirming some hypotheses and suppositions reported elsewhere [8, 9]. Furthermore, more in-depth analyses and perhaps some molecular simulations are required in order to have a better understanding of other parameters or phenomena influencing film thickness.

## 5 Conclusions

According to the film thickness and tribological results from this research work, it can be concluded that passing direct current through the lubricated contact steel interfaces caused significant alterations in film thickness, CoF and ECR, which were mainly assumed to occur by oil viscosity decrease and tribochemical reaction (surface oxidation).

Particularly, film thickness increased and decreased, respectively, with electric current at different speeds and loads. However, the film thickness reduction by interface electrification was more evident when varying sliding speed. It is postulated that, electrical discharge and breakdown during electrified sliding caused more heating than unelectrified sliding, which promotes reduction of oil viscosity and decreased film thickness as consequence.

Also, film alterations by electricity are associated to steel surface oxidation since the current produces more rapid and potent oxidation of steel surfaces, and consequently, generating oxide-rich (hematite ($\alpha$-$Fe_2O_3$)) products/layer (as confirmed by Raman spectroscopy). The oxide products/layer are formed over the surfaces and covering roughness valleys during sliding, which is assumed to promote the film thickness decrease.

In addition, the ECR results provided insight to confirm the formation of oxide products/layer during sliding. ECR increased or kept almost constant with speed or load under electrification instead of decreasing as expected (ECR should reduce during sliding because real contact area increases by both wear or contact pressure increase). The ECR increase with speed under electrification was ascribed to asperities contact intermittence and surface oxidation while ECR increase with load under electrification was only ascribed to surface oxidation.

Finally, the two-electrode cell-based pin-on-disk test instrumented with ultrasound was effective to measure the film thickness of lubricated interfaces running under boundary and mixed lubrication regimes at different speeds and loads.

## Acknowledgements

Julio A. CAO-ROMERO-GALLEGOS and Oscar A. AGUILAR-ROSAS thank the Mexican National Council of Humanities, Science, and Technology (CONAHCYT) and Tecnologico de Monterrey for the scholarships received for conducting part of this research project. Leonardo. I. FARFAN-CABRERA acknowledges the financial support given by Tecnologico de Monterrey within the Challenge-based research project IJST070-23EG68001 (call 2023) to carry out part of this research work.

## Declaration of competing interest

The authors have no competing interests to declare that are relevant to the content of this article.

## References

[1] He F, Xie G X, Luo J B. Electrical bearing failures in electric vehicles. *Friction* **8**(1): 4–28 (2020)

[2] Muetze A, Binder A. Calculation of influence of insulated bearings and insulated inner bearing seats on circulating bearing currents in machines of inverter-based drive systems. *IEEE Trans Ind Appl* **42**(4): 965–972 (2006)

[3] Farfan-Cabrera L I, Erdemir A, Cao-Romero-Gallegos J A, Alam I, Lee S. Electrification effects on dry and lubricated sliding wear of bearing steel interfaces. *Wear* **516–517**: 204592 (2023)

[4] Cao-Romero-Gallegos J A, Reyes-Avendaño J, Soriano J, Erdemir A, and Farfan-Cabrera L. A pin-on-disc study on the electrified sliding wear of EVs powertrain gears. SAE Technical Paper, No. 2022-01-0320, 2022.

[5] Lee P M, Sanchez C, Frazier C, Velasquez A, Kostan T. Tribological evaluation of electric vehicle driveline lubricants in an electrified environment. *Frontiers in Mechanical Engineering* **9**: 1215352 (2023).

[6] El Mansori M, Paulmier D, Ginsztler J, Horvath M. Lubrication mechanisms of a sliding contact by simultaneous action of electric current and magnetic field. *Wear* **225–229**: 1011–1016 (1999)

[7] Holweger W, Schwedt A, Rumpf V, Mayer J, Bohnert C, Wranik J, Spille J, Wang L. A study on early stages of white etching crack formation under full lubrication conditions. *Lubricants* **10**(2): 24 (2022)

[8] Spikes H A. Triboelectrochemistry: Influence of applied electrical potentials on friction and wear of lubricated contacts. *Tribol Lett* **68**: 90 (2020)

[9] Xie G X, Guo D, Luo J B. Lubrication under charged conditions. *Tribol Int* 84: 22–35 (2015)

[10] Xu X, Spikes H. Study of zinc dialkyldithiophosphate in di-ethylhexyl sebacate using electrochemical techniques. *Tribol Lett* **25**(2): 141–148 (2007)

[11] Gangopadhyay A, Paputa Peck M C, Simko S J. Wear control in a lubricated contact through externally applied electric current. *Tribol Trans* **45**(3): 302–309 (2002)

[12] Tung S C, Wang S S. *In-situ* electro-charging for friction reduction and wear resistant film formation. *Tribol Trans* **34**(4): 479–488 (1991)

[13] Wang S S, Maheswari S P, Tung S C. The nature of electrochemical reactions between several zinc organodithiophosphate antiwear additives and cast iron surfaces. *Tribol Trans* **32**(1): 91–99 (1989)

[14] Bouchoucha A, Chekroud S, Paulmier D. Influence of the electrical sliding speed on friction and wear processes in an electrical contact copper–stainless steel. *Appl Surf Sci* **223**(4): 330–342 (2004)

[15] Chiou Y C, Lee R T, Lin S M. Formation mechanism of electrical damage on sliding lubricated contacts for steel pair under DC electric field. *Wear* **266**(1–2): 110–118 (2009)

[16] Becker A, Abanteriba S. Electric discharge damage in aircraft propulsion bearings. *Proc Inst Mech Eng Part J J Eng Tribol* **228**(1): 104–113 (2014)

[17] Esmaeili K, Wang L, Harvey T J, White N M, Holweger W. Electrical discharges in oil-lubricated rolling contacts and their detection using electrostatic sensing technique. *Sensors* **22**(1): 392 (2022)

[18] Ahmed Abdalglil Mustafa W, Dassenoy F, Sarno M, Senatore A. A review on potentials and challenges of nanolubricants as promising lubricants for electric vehicles. *Lubr Sci* **34**(1): 1–29 (2022)

[19] Farfan-Cabrera L I, Cao-Romero-Gallegos J A, Lee S, Komurlu M U, Erdemir A. Tribological behavior of H-DLC and H-free DLC coatings on bearing materials under the influence of DC electric current discharges. *Wear* **522**: 204709 (2023)

[20] Cen H, Lugt P M. Film thickness in a grease lubricated ball bearing. *Tribol Int* **134**: 26–35 (2019)

[21] Brix V H. An electrical study of boundary lubrication. *Aircr Eng Aerosp Technol* **19**(9): 294–297 (1947)

[22] McCarthy D M C, Glavatskih S B, Sherrington I. Oil-film thickness and temperature measurements in PTFE and Babbitt faced tilting-pad thrust bearings. *Proc Inst Mech Eng Part J J Eng Tribol* **219**(3): 179–185 (2005)

[23] Zhang F, Ouyang W, Hong H L, Guan Y S, Yuan X Y, Dong G N. Experimental study on pad temperature and film thickness of tilting-pad journal bearings with an elastic-pivot pad. *Tribol Int* **88**: 228–235 (2015)

[24] Dou P, Jia Y P, Zheng P, Wu T H, Yu M, Reddyhoff T, Peng Z X. Review of ultrasonic-based technology for oil film thickness measurement in lubrication. *Tribol Int* **165**: 107290 (2022)
[25] Gohar R, Cameron A. Optical measurement of oil film thickness under elasto-hydrodynamic lubrication. *Nature* **200**(4905): 458–459 (1963)
[26] Spikes H A, Cann P M. The development and application of the spacer layer imaging method for measuring lubricant film thickness. *Proc Inst Mech Eng Part J J Eng Tribol* **215**(3): 261–277 (2001)
[27] Chen Y P, Zhang X D, Zhang P, Liu C X. Lubricant film thickness measurement using fiber-optic Michelson interferometer and fiber-optic displacement sensor. In Proceedings of the 2009 International Conference on Information and Automation. 2009: 951–956.
[28] Marx N, Guegan J, Spikes H A. Elastohydrodynamic film thickness of soft EHL contacts using optical interferometry. *Tribol Int* **99**: 267–277 (2016)
[29] Obert P, Füßer H J, Bartel D. Oil distribution and oil film thickness within the piston ring-liner contact measured by laser-induced fluorescence in a reciprocating model test under starved lubrication conditions. *Tribol Int* **129**: 191–201 (2019)
[30] Drinkwater B W, Dwyer-Joyce R S, and Cawley P. A study of the interaction between ultrasound and a partially contacting solid-solid interface. *Proceedings of the Royal Society A* **452**(1955): 2613–2628 (1996)
[31] He Y, Wang J, Gu L, Zhang C, Yu H, Wang L, Li Z, Mao Y. Ultrasonic measurement for lubricant film thickness with consideration to the effect of the solid materials. *Applied Acoustics* **211**: 109563 (2023)
[32] Taghizadeh S, Dwyer-Joyce R S. Linear and nonlinear normal interface stiffness in dry rough surface contact measured using longitudinal ultrasonic waves. *Appl Sci* **11**(12): 5720 (2021)
[33] Taghizadeh S, Dwyer-Joyce R S. Influence of asperity deformation on linear and nonlinear interfacial stiffness in dry rough surface contact. *British Society for Strain Measurement*, 2021. Available at https://www.bssm.org/media/of1jrdxs/influence-of-asperity-deformation-on-linear-and-nonlinear-interfacial-stiffness-in.pdf
[34] Rooke J, Brunskill H, Li X W, Taghizadeh S, Hunter A, He S, Lu X Q, Dwyer-Joyce R S. Piston ring oil film thickness measurements in a four-stroke diesel engine during steady-state, start-up and shut-down. *Int J Engine Res* **24**(4): 1499–1514 (2023)
[35] Dwyer-Joyce R S, Reddyhoff T, Zhu J. Ultrasonic measurement for film thickness and solid contact in elastohydrodynamic lubrication. *J Tribol* **133**(3): 1 (2011)
[36] Dwyer-Joyce R S, Drinkwater B W, Donohoe C J. The measurement of lubricant–film thickness using ultrasound. *Proc R Soc Lond A* **459**(2003): 957–976 (2003)
[37] Lu R G, Kawada S, Tani H, Koganezawa S. The influence of electric current on the friction behavior of lubricant molecules. *Tribol Online* **18**(3): 83–90 (2023)
[38] Thomas T R, Sayles R S. Stiffness of machine tool joints. A random process approach. *J. Manuf. Sci. Eng. Trans. ASME* **99**(4): 250–256 (1977)
[39] K. Kendall K and Tabor D. An utrasonic study of the area of contact between stationary and sliding surfaces. *Proc R Soc Lond A* **323**(1554): 321–340 (1971)
[40] Schoenberg M. Elastic wave behavior across linear slip interfaces. *J Acoust Soc Am* **68**(5): 1516–1521 (1980)
[41] Magdun O, Gemeinder Y, Binder A. Investigation of influence of bearing load and bearing temperature on EDM bearing currents. In Proceedings of the 2010 IEEE Energy Conversion Congress and Exposition, Atlanta, GA, USA, 2010: 2733–2738
[42] Aguilar-Rosas O A, Farfan-Cabrera L I, Erdemir A, Cao-Romero-Gallegos J A. Electrified four-ball testing–A potential alternative for assessing lubricants (E-fluids) for electric vehicles. *Wear* **522**: 204676 (2023)
[43] Cao-Romero-Gallegos J A, Farfan-Cabrera L I, Erdemir A, Pascual-Francisco J B. Lubricated sliding wear of gear material under electrification–A new approach to understanding of the influence of shaft currents in the wear of EV transmissions. *Wear* **523**: 204782 (2023)
[44] Zhang J, Spikes H. On the mechanism of ZDDP antiwear film formation. *Tribol Lett* **63**(2): 24 (2016)
[45] Lindgren T, Vayssieres L, Wang H, Lindquist S E. Photo-oxidation of water at hematite electrodes. In: *Chemical Physics of Nanostructured Semiconductors*. Kokorin A I, D. Bahnemann D, Eds. CRC Press, 2003: 83–110.
[46] De Faria D L A, Venâncio Silva S, de Oliveira M T. Raman microspectroscopy of some iron oxides and oxyhydroxides. *J Raman Spectrosc* **28**(11): 873–878 (1997)

**Julio A. CAO-ROMERO-GALLEGOS.** He received his bachelor degree in mechanical engineering (2019) and M.Sc. in nanotechnology (2021) at Tecnológico de Monterrey. By then, he started his Ph.D. studies at the same university. His topic of research is electric vehicles (EVs) tribology, particularly, electrified sliding/rolling metallic contacts and tribochemistry.

**Saeid TAGHIZADEH.** He received his bachelor and master degrees in mechanical engineering (M.Sc. of advanced mechanical engineering at the University of Sheffield, UK). He then has started studying for a fully funded Ph.D. in tribology at the University of Sheffield. He is an expert in measuring and detecting tribological phenomena such as oil film thickness, oil degradation and contamination detection, rheology, contact stiffness, friction and wear. He has been a university teacher, and a postdoctoral research associate in tribology and finite element analysis at the University of Sheffield. One of the main methods he uses for these detections and measurements is linear and nonlinear ultrasound. He also works in the field of machine learning and digital twins of tribology.

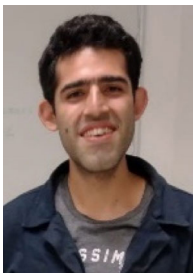

**Oscar A. AGUILAR-ROSAS.** He received his bachelor degree in automotive engineering (2020) and M.Sc. in nanotechnology (2022) at Tecnológico de Monterrey, Mexico. He was visiting scholar at the University of Sheffield and Universidad Politecnica de Valencia, Spain, in 2022.

**R.S. DWYER-JOYCE.** He is director of the Leonardo Centre for Tribology at the University of Sheffield, UK. He has his first degree in mechanical engineering and did his Ph.D. in tribology at Imperial College, UK. He pioneered the use of ultrasound for tribological machine elements, to measure of oil film, contact load, and viscosity. He is a Fellow of the Royal Academy of Engineering, and past editor of the *IMechE Journal of Tribology*.

**Leonardo I. FARFAN CABRERA.** He is Research Assistant Professor and leader of the Automotive and Manufacturing Tribology Lab at Tecnologico de Monterrey, Mexico. He received his M.Sc. and Ph.D. degrees in mechanical engineering at Instituto Politécnico Nacional, Mexico, and was Fulbright Posdoctoral Fellow at Southwest Research Institute (SWRI), USA. His research areas focus on tribology of EVs and automotive components, bio-lubricants, and tribo-testing.